Received: 5 December 2021 | Revised: 13 February 2022 | Accepted: 3 March 2022

DOI: 10.1002/bit.28077

ARTICLE

BIOTECHNOLOGY AND BIOENGINEERING WILEY

Understanding the effects of aerodynamic and hydrodynamic shear forces on *Pseudomonas aeruginosa* biofilm growth

Ye Zhang[1,2] | Dina M. Silva[2] | Paul Young[2,3] | Daniela Traini[2,4] | Ming Li[1] | Hui Xin Ong[2,4] | Shaokoon Cheng[1]

[1]School of Mechanical Engineering, Faculty of Engineering, Macquarie University, Sydney, Australia

[2]Woolcock Institute of Medical Research, Sydney, Australia

[3]Department of Marketing, Macquarie Business School, Macquarie University, Sydney, Australia

[4]Department of Biomedical Sciences, Faculty of Medicine, Health and Human Sciences, Macquarie University, Sydney, Australia

Correspondence

Shaokoon Cheng, School of Mechanical Engineering, Macquarie University, 44 Waterloo Rd., Macquarie Park, Sydney, NSW 2113, Australia.
Email: shaokoon.cheng@mq.edu.au

Hui Xin Ong, Macquarie Medical School, Faculty of Medicine, Health and Human Sciences, Macquarie University, Sydney, NSW 2113, Australia.
Email: huixin.ong@mq.edu.au

Funding information

Macquarie University Research Excellence Scholarship; Marie Bashir Institute

Abstract

Biofilms are communities of bacterial cells encased in a self-produced polymeric matrix and exhibit high tolerance towards environmental stress. Despite the plethora of research on biofilms, most biofilm models are produced using mono-interface culture in static flow conditions, and knowledge of the effects of interfaces and mechanical forces on biofilm development remains fragmentary. This study elucidated the effects of air–liquid (ALI) or liquid–liquid (LLI) interfaces and mechanical shear forces induced by airflow and hydrodynamic flow on biofilm growing using a custom-designed dual-channel microfluidic platform. Results from this study showed that comparing biofilms developed under continuous nutrient supply and shear stresses free condition to those developed with limited nutrient supply, ALI biofilms were four times thicker, 60% less permeable, and 100 times more resistant to antibiotics, while LLI biofilms were two times thicker, 20% less permeable, and 100 times more resistant to antibiotics. Subjecting the biofilms to mechanical shear stresses affected the biofilm structure across the biofilm thickness significantly, resulting in generally thinner and denser biofilm compared to their controlled biofilm cultured in the absence of shear stresses, and the ALI and LLI biofilm's morphology was vastly different. Biofilms developed under hydrodynamic shear stress also showed increased antibiotic resistance. These findings highlight the importance of investigating biofilm growth and its mechanisms in realistic environmental conditions and demonstrate a feasible approach to undertake this study using a novel platform.

KEYWORDS

aerodynamic, biofilm, dual-chamber microfluidic platform, hydrodynamic, interfaces, shear stress

This is an open access article under the terms of the Creative Commons Attribution-NonCommercial-NoDerivs License, which permits use and distribution in any medium, provided the original work is properly cited, the use is non-commercial and no modifications or adaptations are made.
© 2022 The Authors. *Biotechnology and Bioengineering* published by Wiley Periodicals LLC

1 | INTRODUCTION

Biofilms are microbial communities encased within a self-produced extracellular polymeric substance (EPS). The extracellular matrix regulates essential features of the biofilm, such as their adherence to surfaces, hydration, permeability, and tolerance to mechanical forces (Stoodley et al., 2002). The formation of biofilm commences when planktonic bacteria adhere to a surface and forms irreversible attachments. The anchored bacteria multiply and produce EPS, gradually forming a complex 3D biofilm structure that matures over time, which ensues infectious bacteria's dispersal to colonize other areas (Ranganathan, 2014). This biofilm feature enhances their ability to propagate and develop tolerance against adverse conditions, including limited nutrients and when exposed to high concentrations of antimicrobial agents such as biocides, antibiotic and antifungal compounds (Lebeaux et al., 2013).

It has been estimated that 65%–80% of human infections are associated with biofilms, with *Pseudomonas aeruginosa* biofilms as the major cause of many chronic lung infections such as cystic fibrosis, chronic obstructive pulmonary disease, and bronchiectasis (Maurice et al., 2018). Established biofilm infection in the lung is extremely difficult to eradicate. In addition to biofilm's deleterious impact on human health, they also present formidable challenges to many other industries, such as the fouling and corrosion of pipes, which drastically reduce the pipes' life span and present imminent health risks contaminating the water. In agriculture, biofilms may colonize the surfaces and interiors of plants which negatively impact the health and growth of the plant, and this alone is associated with more than 10% of annual loss of global food production (Strange & Scott, 2005).

The growth of biofilms can be affected by the properties of the surfaces they adhere to, such as surface roughness (Cowle et al., 2020), topography (Scheuerman et al., 1998), and hydrophobicity (Callow & Fletcher, 1994). Biofilm proliferation is also likely affected by environmental conditions (e.g., temperature, humidity, and dynamic flow conditions) (Toyofuku et al., 2016), although the detailed effects of these factors on biofilm development remain unclear. In general, there are four different types of interfaces where biofilm develops: air–liquid interface (ALI), liquid–liquid interface (LLI), solid–liquid interface (SLI), and solid–air interfaces (SAI). It is important to model biofilms by considering these interfaces because critical aspects of biofilm developmental processes, such as their attachment, nutrient uptake, mass exchange, are likely incontrovertibly linked to the interfaces. Hence, biofilms proliferating in the respiratory system should be investigated in an ALI environment, whereas biofilms in the urinary tract or interior of the plant should be cultured in LLI. Biofilms in pipes, ship hulls, and medical devices embedded in the sea should be studied using the SLI interface. Moreover, in most of the scenarios, biofilms grow in dynamic conditions where airflow and/or liquid flow are involved. The shear stresses induced by these flows will modulate the development of biofilms.

The majority of experimental biofilm models investigated to date were developed on SLI, and they were cultured using microtiter plate (Peeters et al., 2008), CDC biofilm reactor (Williams & Bloebaum, 2010), rotating disk biofilm reactor (Schwartz et al., 2010), the Calgary Biofilm Device (Ceri et al., 1999) or microfluidic devices (Kim et al., 2010). Only a handful of studies have studied biofilms cultured on LLI, and they are also limited to studying biofilms under static flow conditions (Rühsa et al., 2014). ALI biofilms have previously been produced and studied using the Transwell plate (Woodworth et al., 2008) and the drip flow reactor (Goeres et al., 2009). However, in both systems, understanding the effects of dynamic flow conditions on biofilm growth are challenging. While the Transwell plate can only facilitate biofilm culture under a static flow environment, manipulating airflow rate in the drip flow reactor is limited to a low and small range of flow rates. In general, there remains a significant lack of knowledge of the effects of mechanical shear stresses (induced by airflow and/or hydrodynamic flow) and the multidimensional flow transport mechanisms (e.g., diffusion and convection) of flow medium across different types of interfaces and their comparisons, on biofilms growth and development.

This study aimed to understand the effects of environmental factors specifically, nutrient availability, mechanical shear stress and interface type on the development of biofilm. A dynamic platform was set up in the ALI and LLI configuration using a dual-channel microfluidic device (Ye et al., 2022) for this purpose, with the dynamic system providing a controllable air or liquid flow rate for biofilm culture. We hypothesized that biofilm properties, as determined by the viable cell number, spatial distribution, resistance to physical disruption, permeability, and antibiotic susceptibility to a model antibiotic (ciprofloxacin—CIP) was significantly different between biofilms cultured in ALI and LLI. We further hypothesized that mechanical shear stresses would result in significant changes in biofilm physical structures but could enhance bacteria growth, at least at the surface of the biofilms contacting the dynamic flow.

2 | EXPERIMENTAL METHODS

2.1 | Dual-chamber microfluidic device design and fabrication

A dual-chamber microfluidic device was designed and fabricated to undertake the experiments in this study. The device consists of two polydimethylsiloxane (PDMS) chips containing flow channels separated by an interchangeable membrane. The PDMS chips were mechanically bonded with two plexiglass covers using temporary joints (screws and nuts; Figure 1a). Hence, the device is reversibly bonded to allow reuse and provide flexibility to study biofilm using different interfaces. In this study, the polyester (PETE) membrane was chosen, which is gas permeable and contains hydrophilic pores (PETE 0.2 μm, STELITECH, USA). The design layout of the flow chamber is shown in Figure 1b. The bottom flow channel functions as the media supply channel. The top channel serves as the biofilm culture channel

and has two inlets, one for bacteria inoculation and the other for air or liquid flow to study the effects of dynamic flow conditions on biofilm growth. The PDMS chips were cast using 3-D printing microfluidic techniques, and fabrication details have been illustrated in previous work (Ye et al., 2022).

2.2 | Experimental design and setup for culturing biofilms

2.2.1 | ALI dynamic culture

The design and setup of the microfluidic device platform for culturing biofilm on ALI are presented in Figure 2a. Airflow was generated by an air pump (DC12. OV/370-02PM) and the filter in the pump was sterilized before attaching it to the system. The airflow rate was measured and altered by a valve control flowmeter (LZM6 air gas flow meter with control valve, ABS, China). The syringe pump (Chemyx Fusion 200) provided a continuous media (Cation-adjusted Mueller Hinton Broth [CaMHB], BD Biosciences, Australia) supply in the bottom channel, and the used air and media were collected in waste reservoirs.

2.2.2 | LLI dynamic culture

Two experimental design configurations were used on LLI model to study the effects of hydrodynamic flow-induced shear stresses associated with different flow rates on biofilm development. Figure 2b,c illustrates the experimental setup for biofilms cultured with a low flow rate using a syringe pump (Chemyx Fusion 200) and high flow rate, using a peristaltic pump (Model ISM931A, ISMATEC), respectively.

The assembled microfluidic device was connected to the pump and waste reservoir using Tygong tubing (1.59 mm OD x 0.51 mm ID, Darwin Microfluidics). In the top bacteria inoculation inlet channel, a 22 G blunt needle (Livingstone, Australia) with ends closed was inserted into the tube. The cap of the waste reservoir contained two openings, one for inserting effluent tubes, and the other was connected to a sterile filter to maintain atmospheric pressure in the bottle and to ascertain a sterilized environment. The end of all tubings connected to the waste container was positioned on the same level as the flow channel to maintain consistent pressure in parallel replicates and to minimize pressure differences between the top and bottom channels.

2.3 | System sterilization

All components in the system were sterilized using an autoclave (121°C/20 min) and assembled aseptically in the biosafety cabinet. Before inoculation, 70% ethanol was pumped into the device at a rate of 0.5 ml/min (8×10^{-9} m^3/s) for an hour to clean the channels. The channels in the device were subsequently rinsed with sterile water for another hour. To ascertain that the device was completely sterilized, the flow system was run with sterile CaMHB for 5 min before inoculation, and 100 µl of effluent media was collected from the waste reservoir and plated onto the LB agar plate. To reuse the device, the setup was disassembled after the experiment. All the components were soaked in bleach for 20 min before rinsing with sterile water and sonicated in sterile water for 480 s. All the components were then autoclaved again before the next experiment.

2.4 | Device inoculation

Pseudomonas aeruginosa (PAO1, ATCC 15692, American Type Culture Collection [ATCC]) from frozen stocks were grown on agar plates for 16–18 h at 37°C. The liquid pre-culture was prepared by transferring one PAO1 colony into 1 ml of CaMHB, incubated for 16–18 h at 37°C, and shaken at 200 rotations per minute (RPM). The overnight pre-culture was diluted 1:30 v/v in fresh media, incubated for 2 h at 37°C, and shaken at 200 RPM to make inoculum with $OD_{600} = 0.4$. The consistency of the inoculum size was verified by viable colony forming units (CFU) counts. Before inoculation, the tube for air or liquid flow connected to the top channel was closed with a clamp to avoid contamination, and then a 100 µl inoculum was injected into the top channel through the inoculation needle using a syringe. After inoculation, the entire platform was placed in the incubator at 37°C for 2 h to allow planktonic bacteria to attach to the membrane.

2.5 | The flow rate in biofilm culture

2.5.1 | Biofilm culture on ALI

After bacteria attachment, the inoculum in the top channel was pushed out of the channel by air injected from the inoculation inlet to develop biofilm on the ALI. The tube connected to the other inlet clamped during the inoculation was released to allow airflow through the channel. ALI biofilms were cultured using two different setups: (1) $\tau_w = 0$ Pa condition—air in the top channel was stagnant; (2) $\tau_w \approx 0.3$ Pa condition—airflow rate of 30 ml/min (5×10^{-7} m^3/s) was generated in the top channel. In both the setups, media was infused in the bottom channel at a flow rate of 50 µl/h (1.4×10^{-11} m^3/s).

Flow in the channel was laminar when the associated shear stress, $\tau_w \approx 0.3$ Pa and this is determined by the Reynold number with the following equation (Beirao Da Veiga, 2008),

$$Re = \frac{\rho U D_h}{\mu}, \quad (1)$$

where ρ is the density (Kg/m^3), U is the flow rate (m/s), µ is the dynamic viscosity ($\mu_{air} = 1.66 \times 10^{-5}$ Pa·s, $\mu_{water} = 1.0 \times 10^{-3}$ Pa·s),

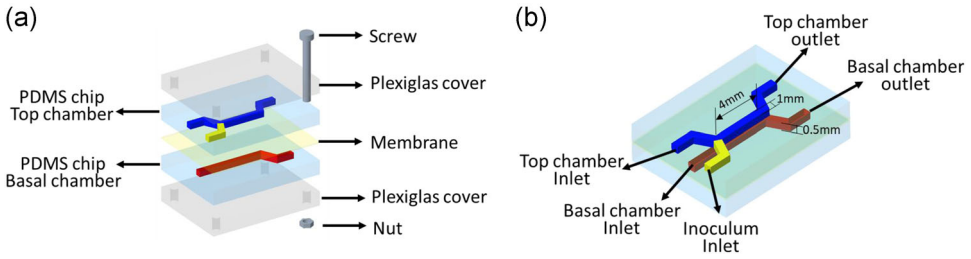

FIGURE 1 (a) Schematic components and assembly of reversible bonding dual-chamber biofilm microreactor; (b) schematic diagram of the design and layout of polydimethylsiloxane flow chambers

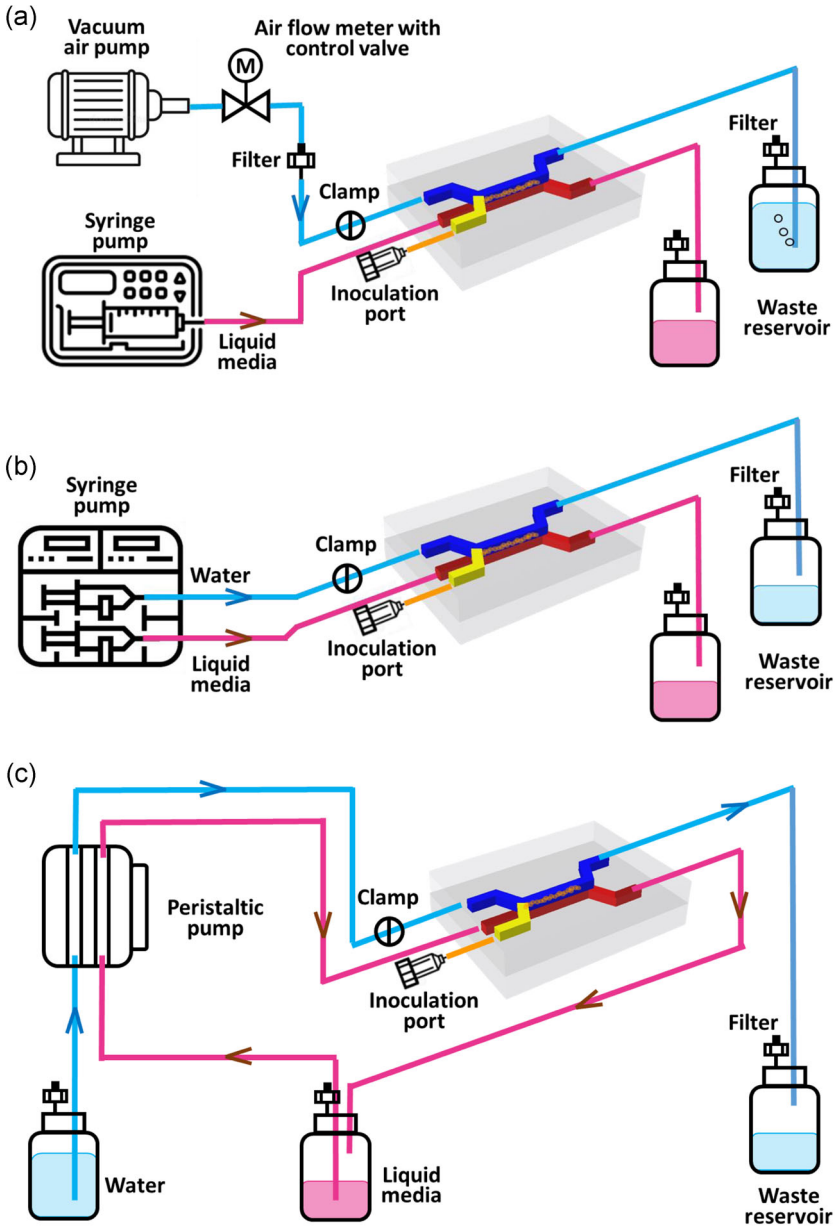

FIGURE 2 Schematic representing the main components of the adaptable microfluidic biofilm culture system. Schematic of air–liquid interfaces dynamic culture system set up (a); schematic of liquid–liquid interfaces dynamic culture system set up for low flow rate (b) and high flow rate (c)

D_h is the hydraulic diameter (m). *Re* was determined as 117 and 11 for the airflow and liquid flow respectively. The mechanical shear stresses at the flow channel walls were calculated using the following equation (Beirao Da Veiga, 2008),

$$\tau_{wall} = \frac{32Q\mu}{\pi {D_h}^3}. \quad (2)$$

Where Q is the flow rate in the channel (m^3/s), μ is dynamic viscosity (Pa·s), D_h is the hydraulic diameter of the channel

(m) (for rectangular channel, $D_h = \frac{4ab}{2(a+b)}$, a is the width, b is the height).

2.5.2 | Biofilm culture on LLI

The biofilms on LLI were also cultured under dynamic flow conditions and the flow rate in the LLI model was determined such that the mechanical shear stress induced by the liquid flow rate matches the airflow rate, and this was achieved to enable a meaningful comparison of biofilms developed on the ALI and LLI. In the case with negligible shear stress ($\tau_w \approx 0$), the top and bottom channels were infused with phosphate-buffered saline (PBS, Sigma Aldrich) and CaMHB media, respectively, at a rate of 50 µl/h (1.4×10^{-11} m^3/s). In the case with $\tau_w \approx 0.3$ Pa, the corresponding flow rate is 0.5 ml/min (8.3×10^{-9} m^3/s). CaMHB (20 ml) was added into the media reservoir and circulated in the bottom channel, and PBS was pumped into the top channel and collected in the waste reservoir. To minimize mass transport across the membrane due to the pressure difference between the two liquid channels, an identical flow rate was maintained in the two channels.

The platform was placed in the incubator at 37°C for biofilm formation for 48 h.

2.6 | Biofilm viable cell number count

The viable bacteria cell number was analyzed at the end of the experiments using colony forming unit (CFU) count. After 48 h culture, membranes containing biofilm samples were picked up from the device, rinsed with 1 ml sterile PBS, and then transferred to a tube containing 1 ml of sterile PBS for 280 s sonication at 47 kHz and 1.8 W/cm^2 to dissolve biofilm bacteria in solutions. Ten-fold serial dilutions of the solution contained rinsed off biofilm bacteria, and the PBS sonicated bacteria suspensions were performed in sterile PBS, plated on LB agar plates, and incubated at 37°C for 16–18 h. Viable colony counts were calculated using the following equation:

$$\text{CFU/ml} = \frac{N \times 10}{10^{-D}}, \quad (3)$$

where N represents the colony number and D represents the number of 1:10 dilutions. The biofilm viability experiments were repeated three times using different batches of inoculum and three samples were collected in each batch.

2.7 | Imaging of biofilm

2.7.1 | Scanning electron microscopy

The biofilms were visualized using scanning electron microscopy (SEM, JEOL, JMC-6000 NeoScope™ Benchtop SEM) at 15 kV. To obtain the SEM images, the devices were disassembled, and membranes were gently rinsed with sterilized water before fixing them in formaldehyde solution in PBS (4% v/v) for 90 min. After fixation, the membranes were rinsed with water and air-dried at 37°C for 1 h. The membranes were sputter-coated with gold for 2 min using a Smart Coater (JEOL) before imaging.

2.7.2 | Confocal laser scanning microscopy

For confocal imaging, the biofilm samples were first stained with FilmTracer™ LIVE/DEAD® (Thermo Fisher Scientific). Next, the images were obtained with a confocal laser scanning microscope (CLSM, Olympus FluoView, inverted FV 3000RS IX83). Before staining, membranes containing biofilm samples were aseptically transferred to a Petri dish and then gently rinsed with 100 µl sterile water followed by staining with 100 µl LIVE/DEAD solution prepared according to the manufacturer instruction for 25 min at 37°C in the dark. Excess dye was removed by rinsing the sample with sterile water. The biofilms were then fixed with 100 µl PFA solution (4% v/v in PBS) for 40 min and rinsed with 100 µl sterile water before mounting them on a glass slide for CLSM imaging. The image was acquired using 488 and 660 nm incident light with a 100× magnification oil immersion objective. The z-stack images were taken with a step of 1 µm with 1024 × 1024 pixels' resolution.

The 3D reconstruction and orthogonal sections of the fluorescence-stained biofilm samples obtained from CLSM z-stack images was obtained using ImageJ software. Biofilm volume was measured using the vortex counter plugin of Image J. The live cells (green) and dead cells (red) were measured separately using the designated color channel. The sum of these two volumes was considered the total volume of biofilm. The thickness of the biofilm sample was measured at 10 locations in both y-z and x-z projection images of orthogonal view of the z-stack image. The averaged thickness and the corresponding standard deviations of the biofilm samples were analyzed from the measurements.

2.8 | Permeability measurement

To investigate the permeability of the biofilms, sodium fluorescein (Na-Flu), a fluorescent probe, was used according to the setup depicted in Figure 3. The end of the outlet tubing in the top and bottom channels was placed 3 cm higher and the same level as the flow cell, respectively. The mechanical pressure at the inlet of the two channels was the same, given that the geometry of the channels and flow rates in the two channels was identical. Thus, the difference in height between the ends of the tubing creates a pressure difference ($\Delta P = \rho g \Delta h$) between the top and bottom channel, and this is likely to drive the flu-Na solution from the top channel to the bottom channel through the biofilm pores. After 48 h of culture, fluorescein sodium (flu-Na) (Sigma Aldrich) solution in PBS (2.5 mg/ml) and pre-warmed PBS were infused into the top channel and the

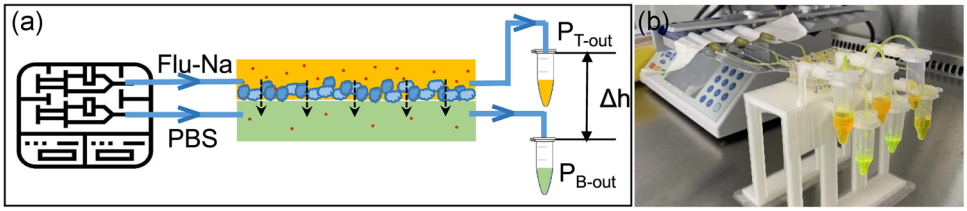

FIGURE 3 (a) Schematic diagram and optical image of the permeability test setup. Flu-Na solution in phosphate-buffered saline (PBS) (2.5 mg/ml) and prewarmed PBS are infused into the top channel and the bottom (acceptor) channel at 100 µl/h, respectively. A 3 cm height difference (Δh) maintained between two outlets creates a constant pressure difference between two chambers (ΔP = PT-out-PB-out = ρg Δh) to drive Flu-Na diffusion. PT-out: pressure at the end of the top channel tube; PB-out: pressure at the end of the bottom channel tube. (b) Photo of the actual experimental setup

bottom channel, respectively, at 100 µl/h and the effluent from the outlet were reserved in the Elfen tubes. Samples of 20 µl effluent from the bottom channel were collected at 15 min, 30 min, 1 h, 2 h, and 4 h. The collected samples were diluted with PBS at a 1:100 volumetric ratio before they were transferred into a black 96-well plate (Corning). The fluorescence intensity was measured by SpectraMax M2 plate reader (Molecular Devices) at excitation and emission wavelengths of 485 and 538 nm, respectively. A linear calibration curve ($R^2 = 0.999$) was obtained between 0.00625 and 12.5 µg/ml concentrations. The apparent permeability coefficient (Papp, cm/s) was calculated using the following equation (Gholizadeh et al., 2021):

$$P_{app} = \frac{dQ}{dt \cdot C_0 \cdot A}, \quad (4)$$

where dQ/dt (µg/s) is the mass flux of the Na-Flu, C_0 (µg/ml) is the initial concentration of flu-Na in the donor compartment, and A (cm^2) is the surface area of the membrane. The permeability assessments were performed on two technical replicates and repeated twice with different bacteria inoculums.

2.9 | Antibiotic susceptibility test

Ciprofloxacin (CIP) is a broad-spectrum antibiotic effective against PAO1 (Brazas & Hancock, 2005) and was used as the model antibiotic in this study. For effective treatment, antimicrobial molecules must diffuse through the biofilm matrix to reach the encased cells. The EPS matrix presents a diffusional barrier for these molecules to kill the bacteria and affects the molecule transport rate (Donlan & Costerton, 2002; Stewart, 2003). To assess the susceptibility of the different biofilm treated with different concentrations of CIP, a stock solution of CIP was prepared in PBS, and working solutions 50, 200, 800, and 1600 µg/ml were freshly prepared by diluting the stock in culture media. The antibiotic solution was injected into the bottom channel using a syringe, and the 48 h-old biofilm was exposed to antibiotics for 6 h at 37°C. The viable cell number was determined after treatment according to the procedure described in Section 2.6. The test was repeated six times (2 technical replicates × 3 biological replicates) for each antibiotic solution concentration.

2.10 | Statistical analysis

Statistical analyses were performed comparing: (1) static versus dynamic continuous nutrient supply ($\tau_w = 0$ Pa), (2) low ($\tau_w = 0$ Pa) versus high ($\tau_w = 0.3$ Pa) shear stresses and (3) ALI vs LLI of the same flow conditions. Data are expressed as mean ± standard deviation (SD). The significance of the difference was determined by a *t*-test. Data sets with a *p*-value less than 0.05 were considered significantly different. All the statistical analysis was performed using Graphpad Prism 7.0. Data of static culture are obtained from Ye et al. (2022).

3 | RESULTS

3.1 | Biofilm viable cell number

The total viable cell number determined by the sum of the bacteria detached from the membrane during rinsing (rinsed) and sonication (sonicated) is represented in Figure 4. Compared to the biofilms cultured under static flow (nutrient-limited) conditions (Ye et al., 2022), the CFUs number with continuous nutrient supply was higher by at least 10-fold in both biofilms formed on ALI or LLI. Under continuous nutrient supply, the mechanical shear stress induced by airflow in the ALI did not show an effect on the average CFUs. However, in LLI culture, the hydrodynamic shear stress ($\tau_w = 0.3$ Pa) significantly reduced the viable CFUs compared to the shear stress-free condition ($\tau_w = 0$ Pa). In addition, with limited nutrient supply (static culture), no significant differences were shown between ALI and LLI biofilm. When LLI biofilms were cultured under continuous nutrient supply, the viable cell number was significantly lower than ALI biofilms. The above suggests the mechanisms in which biofilms uptake nutrients are different when grown on ALI and LLI, with airflow induced shear stress and liquid flow having a different impact on biofilm development.

3.2 | Biofilm adhesive strength

The adhesive strength of biofilms is defined as their resistance to detach by external forces (Ohashi & Harada, 1994; Rutter et al., 1984).

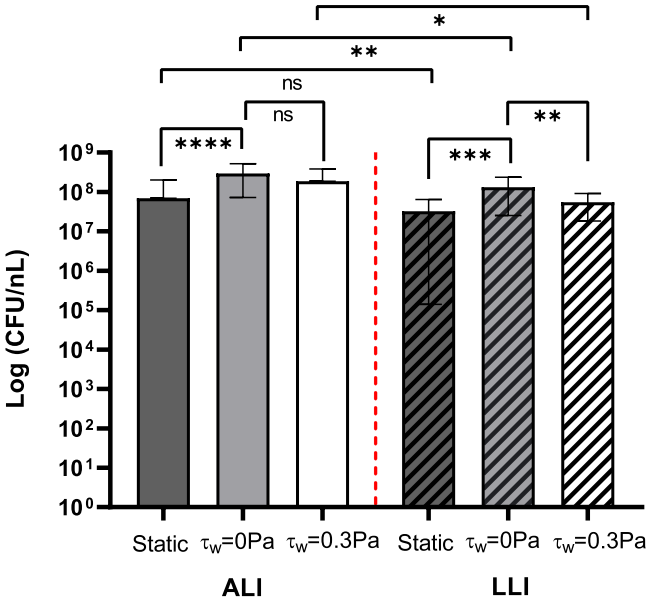

FIGURE 4 The number of viable cells in biofilm samples counted after 48 h culture under various growth conditions (static, negligible shear stress, τ_w = 0.3 Pa). *N* = 18, mean ± SD. The significant difference is shown for the indicated comparison (*p < 0.05; **p < 0.01; ***p < 0.001; ****p < 0.0001; ns, no statistical significance). ALI, air–liquid interfaces; LLI, liquid–liquid interfaces

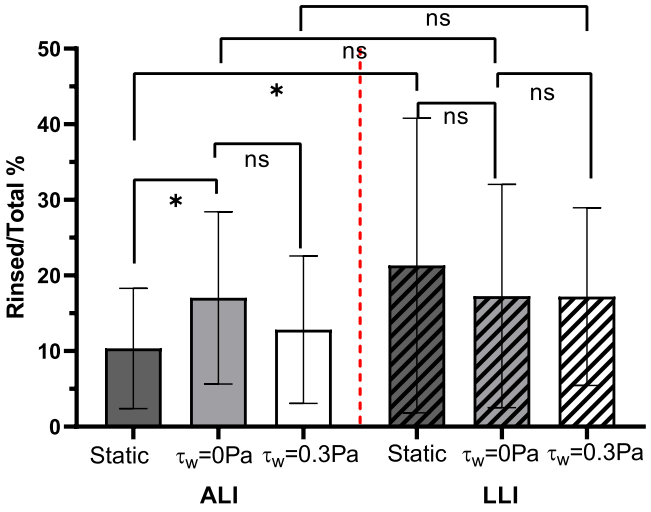

FIGURE 5 The proportion of colony forming units (CFU) number obtained from rinsing solution to the sum of the CFU number obtained from rinsing and sonication solution (*N* = 18, mean ± SD). The significant difference is shown for the indicated comparison (*p < 0.05; ns, no statistical significance. ALI, air–liquid interfaces; LLI, liquid–liquid interfaces

In this study, the adhesive strength of biofilm was analyzed by investigating its resistance to physical disruption, including gentle rinse and strong sonication. The endpoint biofilm samples were gentle rinsed and sonicated. The number of CFUs detached in each step was plated and counted for analysis. The proportion of bacteria number obtained from the rinsing solution to the total bacteria number detached from the membrane (rinsed + sonicated) was compared and shown in Figure 5. Results show that less than 20% of all biofilms were detached from the membrane through rinsing, with the majority of the biofilm detaching by sonication further highlighting the resistant nature of biofilms. ALI biofilm cultured with continuous nutrient supply (τ_w = 0 Pa) showed a decreased resistance to rinsing compared to the biofilm cultured in static flow (nutrient-limited) condition, and this was demonstrated by the higher percentage of rinsed-off bacteria (20%) than biofilm cultured under static conditions (10%). In addition, the mechanical shear stress induced by airflow (τ_w = 0.3 Pa) had no significant impact on ALI biofilm's adhesion strength compared to the biofilm cultured with no shear stress impact (τ_w = 0 Pa). On the other hand, for biofilm cultured on LLI, the adhesive strength of biofilm developed with continuous nutrient supply had no significant change compared to the biofilm developed with limited nutrient supply. Moreover, under continuous nutrient supply, shear force induced by liquid flow (τ_w = 0.3 Pa) had no significant impact on biofilm's adhesive strength. Comparing the biofilm formed on the different interfaces under the same nutrient supply conditions, LLI biofilm showed significant lower adhesive strength compared to ALI biofilm only for the static culture condition.

3.3 | Biofilm morphology

SEM images (Figure 6) show that biofilms cultured with continuous broth supply generally constitute a dense and compacted multilayer structure, suggesting that the bacteria had multiplied successfully and was tightly bonded. It can be observed that the surface of ALI biofilms cultured in dynamic flow conditions was smooth and homogenous (Figure 6a,b). However, LLI biofilms display remarkably different surface morphology when cultured under different dynamic flow conditions (Figure 6a). Mechanical shear stress appears to produce LLI biofilms with a more rippled surface (Figure 6c). More specifically, an increase in mechanical shear stresses (τ_w = 0.3 Pa) in the LLI culture appears to produce a more heterogeneous biofilm showing notable ridges and dome-shaped structures (Figure 6d). These morphology differences were also displayed in CLSM images (Figure 7). These results demonstrate that the impact of mechanical shear stress is likely greater on the LLI biofilm surface than on the ALI biofilm for the range of flow rates and mechanical shear stresses conducted in this study.

The biofilm average thickness, volume, and live-cell spatial distribution analyzed from the CLSM images are shown in Figure 8. Analysis showed that ALI biofilm developed with continuous nutrient supply and under negligible shear stress (τ_w = 0 Pa) was four times thicker than the ALI biofilm developed under static flow (nutrient-limited) conditions. On the other hand, the LLI biofilm with negligible shear stress (τ_w = 0 Pa) was two times thicker than the LLI biofilm developed under static flow (nutrient-limited) conditions. It was also twofold thinner than the ALI biofilm culture with negligible shear stress (τ_w = 0 Pa). Higher mechanical shear stress (τ_w = 0.3 Pa) had obvious and different effects on the thickness of ALI and LLI biofilms.

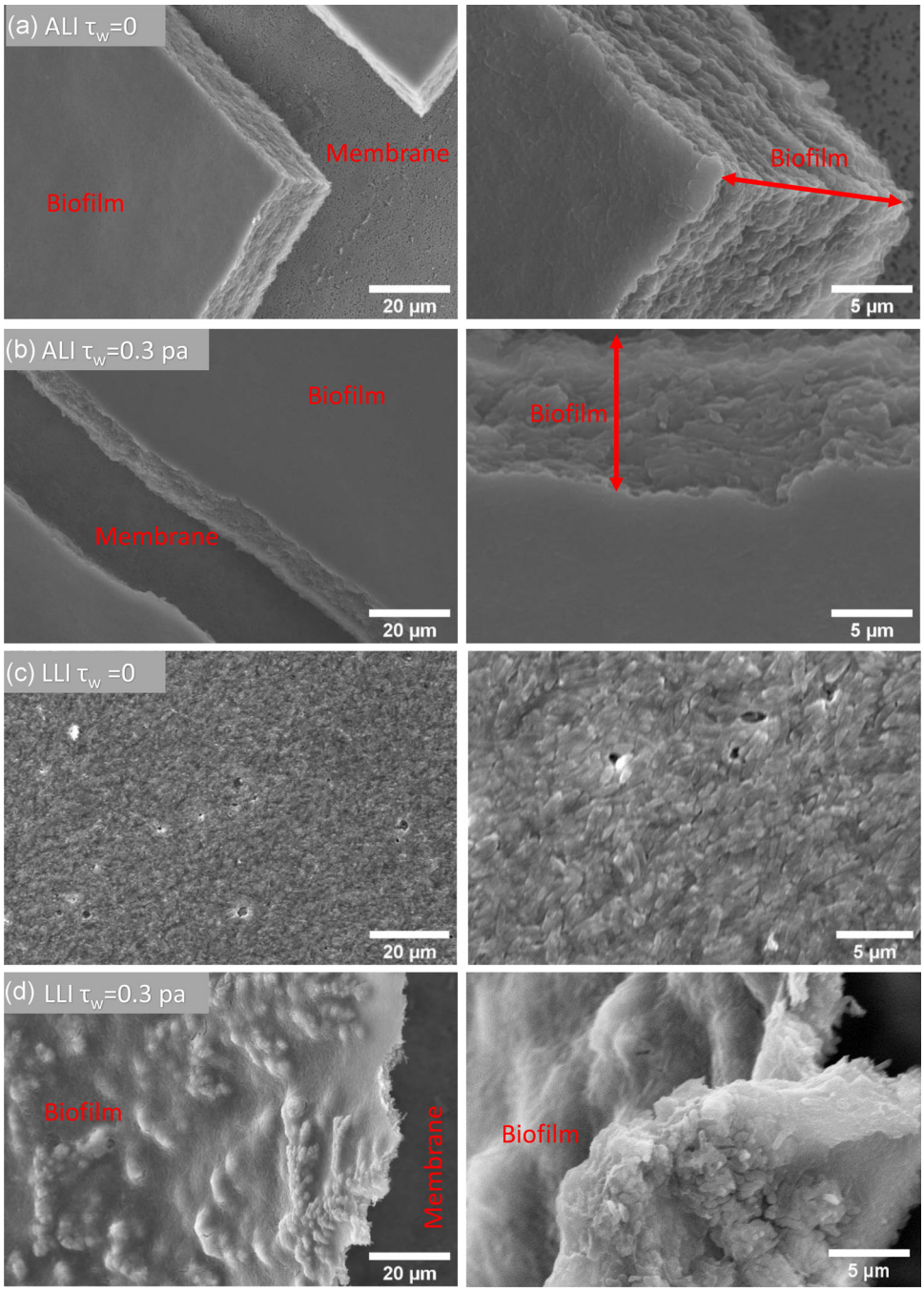

FIGURE 6 Representative scanning electron microscopy images of biofilms cultured on air–liquid interfaces and liquid–liquid interfaces under different shear force conditions. ALI, air–liquid interfaces; LLI, liquid–liquid interfaces

In the ALI biofilm, mechanical shear stress (τ_w = 0.3 Pa) resulted in a biofilm of 30 μm, 25% thinner than the ALI biofilm developed under negligible shear stress (τ_w = 0 Pa). On the other hand, the LLI biofilm developed under hydrodynamic shear stress (τ_w = 0.3 Pa) was only 5% thinner than the LLI biofilm cultured under negligible shear stress (τ_w = 0 Pa) and 45% thinner than the ALI biofilm (τ_w = 0.3 Pa). Hence, ALI biofilms were significantly thicker than LLI biofilms when cultured under the same nutrient condition, with ALI being significantly affected by the increase in shear stresses than the LLI biofilm.

The volume of bacteria (live and dead) encased in the biofilm structure was measured and compared in Figure 8b. It showed that most of the bacteria (up to 90%) were alive in all conditions. The continuous supply of nutrients is likely to have accelerated biofilm proliferation, and this is represented by a significantly larger bacteria volume than the biofilm cultured in static flow (nutrient-limited) conditions. Bacteria volume is directly related to the bacteria number and the larger the CFU number, the larger the bacteria volume. Hence, bacteria volume is expected to correspond with CFU measurements such that larger bacteria volume should be associated

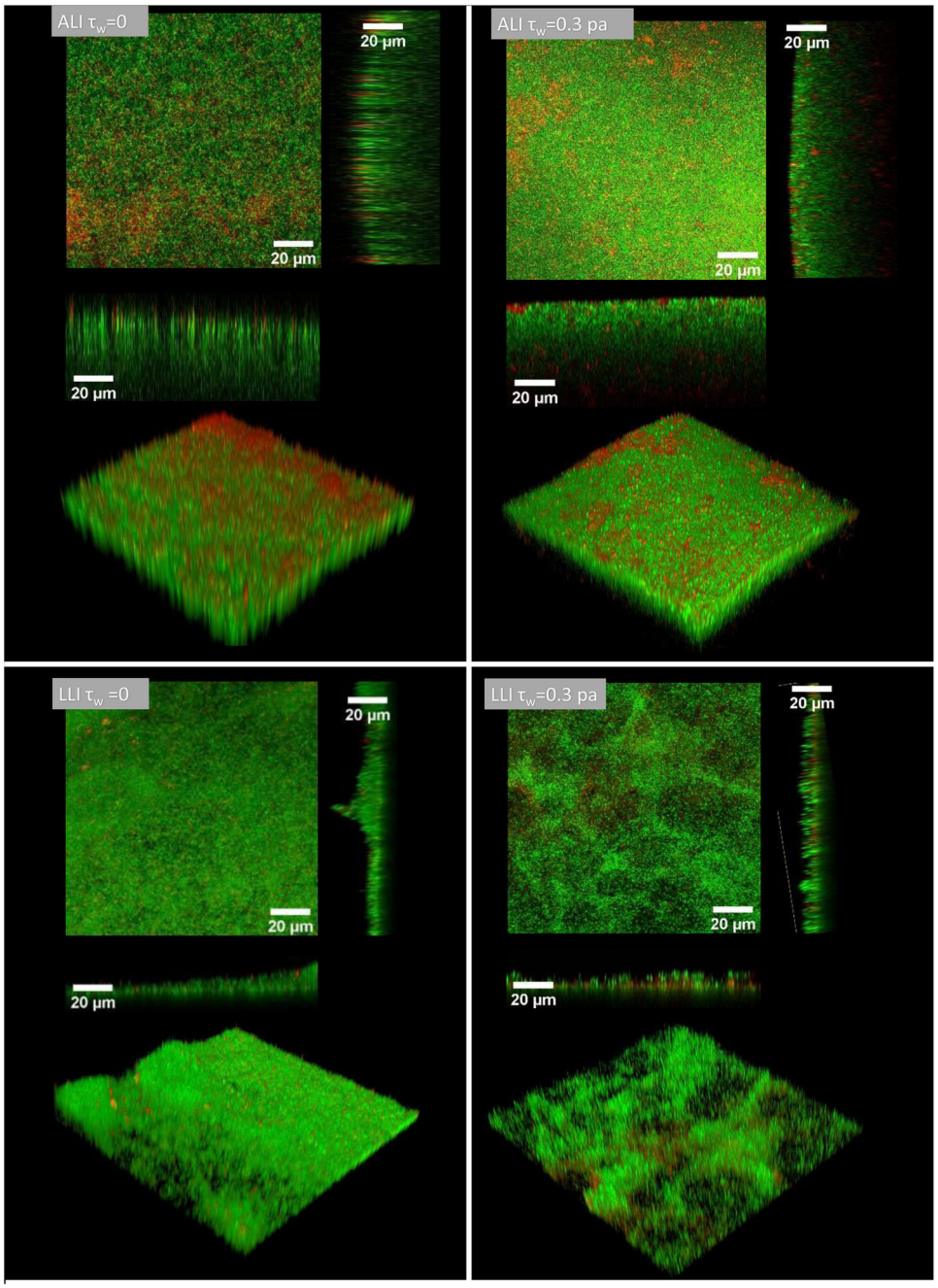

FIGURE 7 Representative confocal laser scanning microscope images of biofilms cultured on air–liquid interfaces and liquid–liquid interfaces under different dynamic conditions. Images are displayed by orthogonal view and 3D-reconstruction view of the z-stack image

with a higher CFU number. Our CFU count results (Figure 4) and bacteria volume (Figure 8b) measured from CLSM images agree with each other.

Figure 8c shows the spatial distribution of live cells across the biofilm thickness from the side attaching the membrane to the biofilm surface. The live-cell distribution is represented by the proportion of live-cell volume to total bacteria volume. The results showed that the trend of live-cell changes across the biofilm thickness was similar for the ALI biofilms cultured under static flow and dynamic but negligible shear stress (τ_w = 0 Pa) conditions. ALI biofilms cultured under these conditions had the largest live-cell proportion (≈100%) of the membrane surface. The number of live cells reduced exponentially as a function of the biofilm thickness and was only ~20% at the outer surface of the biofilm. Mechanical shear stress (τ_w = 0.3 Pa) appeared to have an obvious effect by changing the profile of the live cells across the biofilm thickness. The higher mechanical shear stresses produced a pseudo constant live-cell distribution of ~80% between 0.2 and 0.8 of the normalized biofilm thickness measured from the membrane attaching side. The live cells proportion decreased from 75% at 0.95 of the normalized biofilm thickness to 45% close to the biofilm's surface.

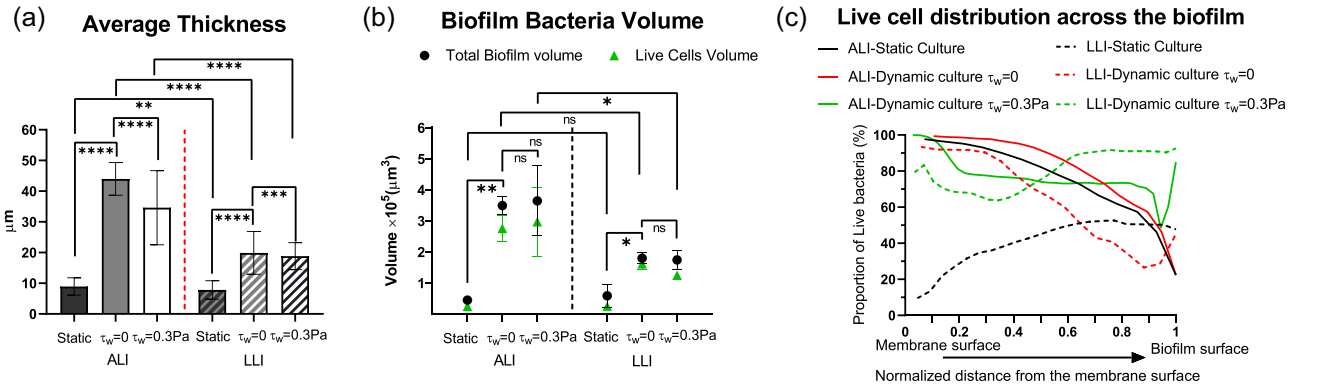

FIGURE 8 Comparison of (a) averaged thickness; (b) biofilm bacteria volume; (c) live cell distribution across the biofilm layer ($N = 6$, mean ± SD). The significant difference is shown for the indicated comparison (*$p < 0.05$; **$p < 0.01$; ***$p < 0.001$; ****$p < 0.0001$; ns, no statistical significance)

The effects of mechanical shear stress on the LLI biofilm are more complex, demonstrating that environmental conditions significantly impact the biofilm developmental process. The results showed that for LLI biofilms cultured in static flow (nutrient-limited) conditions, the live bacteria distribution profile was 10% at the membrane side but 50% at the external surface of the biofilm. It is highly plausible that the low adhesive strength of the LLI biofilm cultured under static flow (nutrient-limited) conditions were related to the fact that it had the smallest proportion of live-bacteria on the membrane side. The opposite behavior was observed for ALI biofilms cultured under the same static conditions that showed a decreasing viability across the thickness of the biofilm. On the other hand, LLI biofilms under dynamic conditions with induced negligible shear stress was sufficient to change the live-cell distribution profile completely. With dynamic flow conditions ($\tau_w = 0$ Pa), the proportion of live cells is 90% at the membrane side, 20% at 0.9 of the normalized biofilm thickness and 45% at the biofilm's surface. An increase in mechanical shear stress ($\tau_w = 0.3$ Pa) also had an apparent effect on the proportion of live cell distribution profiles. The live-cell proportion at the biofilm's surface was higher at 90% and twofold higher than the LLI biofilm cultured with negligible shear stress. The above results are likely related to the changes in mass transfer at the interfaces of two-phase shear-flow due to differences in hydrodynamic forces, and extended work using computational fluid dynamics is useful to elucidate the intricate mechanisms underpinning the processes.

3.4 | Biofilm permeability

Figure 9 shows the P_{app} of determined for empty membrane (control) and membrane with biofilms attached using the Na-Flu assay. Compared to the empty porous membrane, biofilm formation reduced its permeability by at least 50%. Both ALI and LLI biofilms developed under continuous nutrient supply conditions with negligible shear stress ($\tau_w = 0$ Pa) had lower permeability than those developed under static (nutrient-limited) conditions, and the differences were significantly larger for the ALI biofilm than the LLI Biofilm. Inducing higher mechanical shear stresses ($\tau_w = 0.3$ Pa) by increasing the flow rates reduced the permeability significantly in

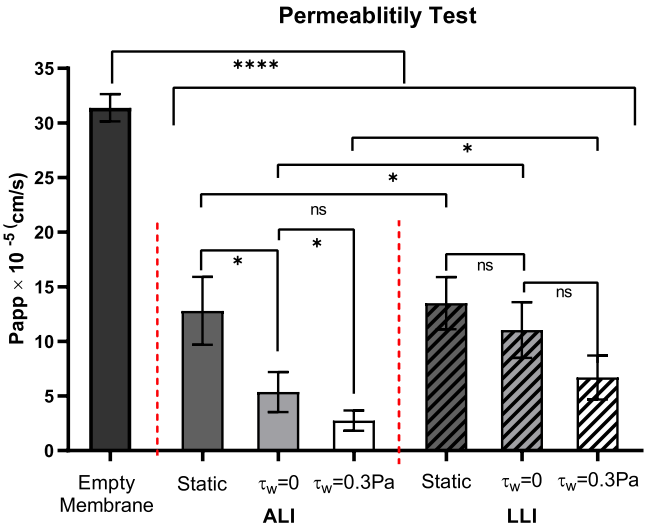

FIGURE 9 The permeability coefficient determined the membrane without biofilm (control) and the membrane with the biofilm cultured on air–liquid interfaces (ALI) and liquid–liquid interfaces (LLI) under 48 h static and dynamic conditions using the Flu-Na paracellular permeability marker ($N = 4$, mean ± SD). The significant difference is shown for the indicated comparison (*$p < 0.05$; ****$p < 0.0001$; ns, no statistical significance)

the ALI biofilms but not significantly in the LLI biofilm. Under continuous nutrient supply conditions, the LLI biofilm's permeability was at least twofold higher than the ALI biofilms. The results indicate that mechanical shear stress is likely able to affect biofilm permeability, given the wide range of permeability measurements obtained from the biofilm cultured in different environmental conditions and interfaces explored in this study.

3.5 | Antibiotic susceptibility test and minimum biofilm eradication concentration measurements

The percentage of bacteria after antibiotic treatment compared to the control group is shown in Figure 10. Compared to biofilm

cultured in static (nutrient-limited) conditions, generally, the percentage of live bacteria was 10–100 times higher for the biofilm cultured with continuous nutrient supply after exposure to the same antibiotic concentration. The percentage of survived bacteria of all the biofilms cultured under dynamic flow conditions dropped steadily when antibiotics concentration increased from 50 to 800 μg/ml but was unchanged when the antibiotic concentration increased further from 800 to 1600 μg/ml. However, biofilms cultured under static flow (nutrient-limited) conditions showed a gradual and consistent drop in the surviving bacteria with increased antibiotic concentration. These results indicate that biofilm cultured with continuous nutrient supply is more resistant to antibiotics compared to static culture. In dynamic ALI culture, the shear stress (τ_w = 0.3 Pa) induced by airflow had no significant impact on ALI biofilm's antibiotic susceptivity. However, in LLI dynamic culture, hydrodynamic shear stress (τ_w = 0.3 Pa) produced biofilm with increased antibiotic resistance compared to biofilm cultured under negligible stress conditions (τ_w = 0 Pa). In addition, no significant differences were shown between the biofilm cultured on ALI and LLI under the same nutrient and shear stress conditions.

The minimum biofilm eradication concentration (MBEC) is commonly defined as the lowest concentration of an antimicrobial substance needed to eradicate 99.9% of biofilm-embedded bacteria (3 log10 reductions in CFU/ml) compared to growth controls in the same conditions (Barry, 1999; Thieme et al., 2019). Based on this definition, the MBEC for biofilm cultured under static flow condition was 200 μg/ml. This value is greater for the dynamic cultured biofilm, which is 1600 μg/ml.

4 | DISCUSSION

Understanding how biofilm properties may be affected by different environmental conditions such as determining the effects of airflow and hydrodynamic flow-induced shear forces on biofilm growth is important to inform the development of effective biofilm eradication strategies. To the best of the authors' knowledge, this study presents the first comparison of ALI and LLI biofilms cultured using flow conditions associated with mechanical shear stresses of the same magnitude. While the superficial appearances of biofilms cultured under different conditions appear similar under visual inspection, results from the analysis provide clear evidence that biofilm's developmental process and structure is dramatically different when cultured on ALI and LLI, with dynamic flow conditions having significant effects on various aspects of biofilms' properties and especially on the permeability, morphology, and proportion of live cells distribution profile across the biofilm thickness. Furthermore, compared to LLI biofilms subjected to hydrodynamic forces, this study shows that ALI biofilms exposed to dynamic airflow result in thicker, denser, but less permeable biofilm with more homogenous surfaces.

4.1 | Nutrient-related biofilm developed on ALI and LLI (static culture vs. dynamic culture τ_w = 0 Pa)

Using a dual-channel microfluidic device, biofilms were cultured under static flow or dynamic flow conditions and replicated a nutrient

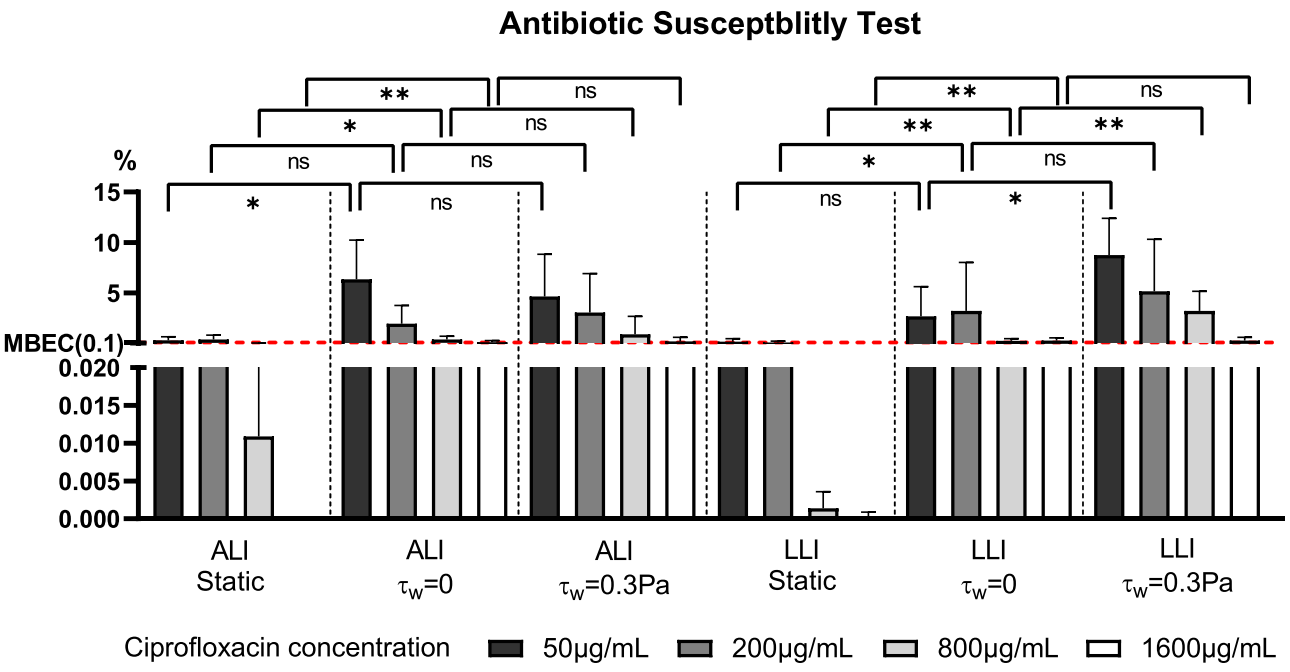

FIGURE 10 Comparison of biofilm eradication effect of ciprofloxacin (50, 200, 800, and 1600 μg/ml) for 6 h exposure on 48 h-old biofilms cultured under different conditions. Antibiotic exposure was performed from the basal chamber (N = 6, mean ± SD). The red dash line indicates the MBEC level. The significant difference is shown for the indicated comparison (*p < 0.05; **p < 0.01; ns, no statistical significance). ALI, air–liquid interfaces; LLI, liquid–liquid interfaces; MBEC, minimum biofilm eradication concentration

limiting environment (Ye et al., 2022) or an environment where nutrients are supplied continuously. As demonstrated in this study, the distinct difference in biofilm's physical properties obtained from these two different culture methods (static vs. dynamic flow) shows that nutrient supply plays an important role in biofilm growth. While several existing studies have reported the effect of nutrients and showed how high nutrient concentration promotes biofilm growth (Cunningham et al., 1991; Liu et al., 2019; Stoodley et al., 1998; Vandevivere & Baveye, 1992), our study shows further that with continuous nutrient supply, bacteria proliferated within 48 h, and this time frame is sufficient to form significantly thicker and denser biofilms with lower permeability that has higher antibiotic tolerance compared to the biofilms cultivated under nutrient-limited conditions. Such information is not only useful to estimate the time of biofilm establishments in an ALI and LLI environment but it can also be used to predict biofilm properties, including their susceptibility to eradication for a given antibiotic concentration. Liu et al. (2019) demonstrated that biofilm cultured on SLI with high nutrient concentration has weak adhesive strength. However, our study shows that ALI biofilms cultured under continuous nutrient supply has reduced adhesive strength, but this is not observed in LLI biofilms. The above may be related to the difference in nutrient transportation mechanisms associated with different interfaces. Our results further show that biofilms developed with continuous nutrient supply are 10–100 times more resistant to antibiotics than those cultured under limited nutrient conditions. In addition, the MBEC for continuously nurtured biofilm is 8 times higher than mal-nourished biofilm. This is because biofilm cultured with continuous nutrient supply produced more EPS content that effectively protects encased cells against the antimicrobials.

4.2 | Interface-related effects—ALI biofilms versus LLI biofilms

Under dynamic conditions, the biofilms formed on ALI and LLI developed remarkably different structures with LLI biofilms producing significantly lower viable bacteria numbers. The differences are due to the different environmental impacts on the biofilm-forming process when growing on different interfaces. In ALI, the matured biofilm exposed to the air is less likely to be detached from the developed biofilm structure. However, detachment is facilitated in LLI since bacteria can move more freely in the liquid submerged environment. Thus, the LLI biofilm structure is constantly changing in the fluid environment resulting in more heterogeneous structures and fewer bacterial cell numbers compared to ALI biofilm.

Differences in biofilm's permeability and live-cell distribution between the ALI and LLI biofilms are likely related to differences in mass transfer mechanisms across the interfaces. In this study, the dual-channel microfluidic device is separated by a hydrophilic porous and permeable membrane. The pressure in the channel induced by airflow is lower than the membrane's bubble point (Hydrophilic Polyester Track Etch PETE Membranes Specification, 2016), which means that air is unlikely to pass through the membrane to the channel containing the media. It has been well recognized that biofilm structures are interspersed with water channels for nutrient transport and waste expel (Costerton, 1995; Stoodley et al., 1994). Yang et al.'s study (Yang & Lewandowski, 1995) suggest that in these heterogeneous distributions of internal water channels, transportation of nutrients in the channels are likely driven by a convective term in addition to molecular diffusion. In this study, the top and bottom channel in the microfluidic device is connected by the membrane pores. Hence, it is not difficult to envisage that the transportation of nutrients via molecular diffusion and convection is facilitated in the LLI experimental configuration and less in the gas-liquid configuration. This may explain why LLI biofilm develops as a more permeable and porous structure, with presumably larger water channels. Another plausible evidence supporting this hypothesis is that the live bacteria proportion is constant across the LLI biofilm thickness in continuous media supply, further supporting the concept that the LLI biofilm is saturated with media, facilitating larger mass transport across the membrane and the biofilm compared to the ALI biofilm. The biofilm growth on ALI and LLI showed no significant difference in antibiotic susceptibility. Given the obvious change in live-cell distribution and differences in physical properties of the biofilms, the reason for this is unclear and could be related to the mechanisms of actions in the antimicrobials, such as their limited ability to eradicate certain constituents of the biofilm. This is supported by the observation that the trend of continuous improvement in biofilm eradication with higher antimicrobial concentration is only observed for biofilms cultured in nutrient-limited conditions. These results suggest that MBEC of an antibiotic should be tested by first considering the number of nutrients supplied to the biofilms of interest during the drug development phase given that the improper management of biofilms through the use of inadequate antimicrobial may lead to super-resistant bacteria (Stewart, 2002).

4.3 | Mechanical shear stress-related biofilm

This study shows that mechanical shear stress has a significant impact on biofilm growth and its properties. It does not significantly affect bacteria count in ALI but results in significantly lower CFU counts in an LLI biofilm culture. Mechanical shear stress also appears to have a significant impact on biofilm thickness, density, permeability, and the proportion of live-cell distribution across the biofilm. Previous studies demonstrated that biofilms exposed to hydrodynamic shear forces are thin, have heterogeneous structures (Stoodley et al., 1998; Vieira et al., 1993), and have high adhesive strength (Chen et al., 1998). Our findings show that they not only correspond well with the existing work, but we further show that such properties are also associated with significantly lower permeability across the LLI biofilm. Furthermore, Hassanpourfard et al. (2016) demonstrated that hydrodynamic stresses could detach portions of biofilm, leading to extended water channels in developed structures. Hence, it is plausible that the lower permeability observed

in our LLI biofilm at the higher shear stress is related to the distortion of water channels, which has increased mass transport resistance.

Mechanical shear stress is ubiquitous in biological processes, with airflow in human lungs being a common example. During respiration, shear stresses in a representative Horsfield generation 10 region (the generation number commonly used in a symmetrical dichotomously branching system) (Horsfield & Cumming, 1968) ranges from -4×10^{-3} to 4×10^{-3} cmH_2O (0–0.4 Pa) (Nucci et al., 2003). The impact of airflow-induced shear stress of this magnitude is investigated in our study. We show that biofilms developed under such conditions are different from biofilms exposed to hydrodynamic shear stress of the same magnitude. The increase in airflow induced shear stress produced biofilms that are thinner, denser, and less permeable compared to their controls cultured under shear stress negligible conditions. The increase in shear stress is also associated with changes in live-cell distribution across the biofilm thickness, especially at the outer surface, and this may be related to the biofilm being exposed to more oxygen from the higher airflow rate. It is also interesting to note that biofilm shows more homogenous planar morphology when developed under the influence of airflow. In addition, there is no significant difference in the resistance of ALI biofilms against antimicrobials, at least based on the range of shear stress investigated in this study. The effect of higher mechanical shear stress on LLI biofilms is distinctively different from the ALI biofilms. This can be readily observed in the viable CFU counts, live bacteria distribution across the biofilm and biofilm's antibiotic susceptibility. Higher hydrodynamic shear stress appears to reduce viable cell number, homogenize the distribution of live cells across the biofilm, and increase antibiotic resistance. While there appear to be insignificant changes in biofilm volume with increased hydrodynamic shear stress, extended studies to delineate the potential effects for a wider range of shear stress magnitude (e.g., in orders of magnitude) comprehensively and as a function of culturing time is warranted to improve knowledge of the mechanisms of biofilm growth in a dynamic environment.

While biofilms have been widely studied, how these microorganisms thrive in dynamic mechanical environments remains unclear. Being able to understand the impact of mechanical forces and, specifically, how they may change the properties of biofilm over time would be extremely useful for a wide range of engineering applications from the perspective of developing novel products to control, monitor their growth. The above knowledge will also pave the way to enable the development of effective eradication strategies to treat biofilms.

4.4 | Limitations

Despite the new findings obtained from this study, there are several inherent limitations in the experimental study design. First, the impact of mechanical shear stress has been investigated within the same order of magnitude. As discussed, future work is warranted to explore the effects and implications for a wider range of mechanical shear stress. Second, high shear flow LLI biofilm cultured using a high flow rate was achieved using a peristaltic pump because the syringe pump was unable to handle the large volume of liquid associated with the high flow rate cases. However, it is important to note that the concern where the peristaltic pump may have supplied a higher level of nutrient due to recirculation of the CaMHB media is negligible given that the volume of nutrients that biofilm is exposed to during its course of growth is constant (determined by the volume of the bottom flow chamber), and the change of the media concentration is negligible considering the small volume of biofilm sample. Third, the flow rate provided by the peristaltic pump is pulsatile, which is not constant compared to the airflow provided by the syringe pump. However, implications of this are likely minor as the frequency of pulsation is high. However, in-depth studies exploring the effects of pulsatile flow conditions are warranted as they are useful to shed light on how such dynamic flow condition alters biofilm properties common in infectious lung diseases. In addition, EPS plays an important role in biofilm surface adhesion. Unfortunately, the properties of the EPS and quantifying whether they are loose or dense have not been thoroughly investigated as it was not defined as a study's scope in this current work. Future work to include the investigation of these changes may shed more insights on biofilm growth behavior. Finally, different bacterial strains are likely to exhibit different growth trends in a given environmental condition. So far, we have studied PAO1, and further plans are currently underway to investigate the growth properties of other strains such as *Escherichia coli*, *Staphylococcus aureus* in biofilm formation. It would also be interesting to further study their co-growth behavior, which is ubiquitous in nature and represents how biofilm usually grows and thrive realistically.

5 | CONCLUSIONS

The dual-channel microfluidic platform developed to investigate biofilm development in this study has been demonstrated as a successful in vitro tool to emulate biofilm growth in a realistic physiobiological environment. Discoveries from this study support the need to develop innovative approaches to characterize biofilms and their phenotypes longitudinally based on their physical properties, such as cell density, thickness, permeability, and mechanical properties, an approach that could potentially enhance our overall understanding of biofilms.

AUTHOR CONTRIBUTIONS

The project was conceptualized by Shaokoon Cheng, Hui Xin Ong, and Ye Zhang. Experiments conduction and data analysis were performed by Ye Zhang with advice and supervision by all co-authors. The manuscript was written by the first author with review and edit from all co-authors.

ACKNOWLEDGMENTS

This study was supported by Marie Bashir Institute and Macquarie University Research Excellence Scholarship. The authors would also like to thank the Microscopy Unit of Macquarie University. Open access publishing facilitated by Macquarie University, as part of the Wiley - Macquarie University agreement via the Council of Australian University Librarians.

CONFLICTS OF INTEREST

The authors declare no conflicts of interest.

DATA AVAILABILITY STATEMENT

The data that support the findings of this study are available from the corresponding author upon reasonable request.

ORCID

Ye Zhang https://orcid.org/0000-0002-6244-1173
Ming Li https://orcid.org/0000-0001-7450-6205

REFERENCES

Barry, A. L. (1999). *Methods for determining bactericidal activity of antimicrobial agents: Approved guideline*. National Committee for Clinical Laboratory Standards.

Beirao Da Veiga, H. (2008). *Fluid dynamics*. Springer.

Brazas, M. D., & Hancock, R. E. W. (2005). Ciprofloxacin induction of a susceptibility determinant in *Pseudomonas aeruginosa*. *Antimicrobial Agents and Chemotherapy*, *49*(8), 3222–3227. https://doi.org/10.1128/AAC.49.8.3222-3227.2005

Callow, M. E., & Fletcher, R. L. (1994). The influence of low surface energy materials on bioadhesion—A review. *International Biodeterioration & Biodegradation*, *34*(3), 333–348. https://doi.org/10.1016/0964-8305(94)90092-2

Ceri, H., Olson, M. E., Stremick, C., Read, R. R., Morck, D., & Buret, A. (1999). The Calgary biofilm device: New technology for rapid determination of antibiotic susceptibilities of bacterial biofilms. *Journal of Clinical Microbiology*, *37*(6), 1771–1776. https://doi.org/10.1128/JCM.37.6.1771-1776.1999

Chen, M. J., Zhang, Z., & Bott, T. R. (1998). Direct measurement of the adhesive strength of biofilms in pipes by micromanipulation. *Biotechnology Techniques*, *12*(12), 875–880. https://doi.org/10.1023/A:1008805326385

Costerton, J. W. (1995). Overview of microbial biofilms. *Journal of Industrial Microbiology*, *15*(3), 137–140. https://doi.org/10.1007/BF01569816

Cowle, M. W., Webster, G., Babatunde, A. O., Bockelmann-Evans, B. N., & Weightman, A. J. (2020). Impact of flow hydrodynamics and pipe material properties on biofilm development within drinking water systems. *Environmental Technology*, *41*(28), 3732–3744. https://doi.org/10.1080/09593330.2019.1619844

Cunningham, A. B., Characklis, W. G., Abedeen, F., & Crawford, D. (1991). Influence of biofilm accumulation on porous media hydrodynamics. *Environmental Science & Technology*, *25*(7), 1305–1311. https://doi.org/10.1021/es00019a013

Donlan, R. M., & Costerton, J. W. (2002). Biofilms: Survival mechanisms of clinically relevant microorganisms. *Clinical Microbiology Reviews*, *15*(2), 167–193. https://doi.org/10.1128/CMR.15.2.167-193.2002

Gholizadeh, H., Ong, H. X., Bradbury, P., Kourmatzis, A., Traini, D., Young, P., Li, M., & Cheng, S. (2021). Real-time quantitative monitoring of in vitro nasal drug delivery by a nasal epithelial mucosa-on-a-chip model. *Expert Opinion on Drug Delivery*, *18*, 1–16. https://doi.org/10.1080/17425247.2021.1873274

Goeres, D. M., Hamilton, M. A., Beck, N. A., Buckingham-Meyer, K., Hilyard, J. D., Loetterle, L. R., Lorenz, L. A., Walker, D. K., & Stewart, P. S. (2009). A method for growing a biofilm under low shear at the air–liquid interface using the drip flow biofilm reactor. *Nature Protocols*, *4*, 783–788. https://doi.org/10.1038/nprot.2009.59

Hassanpourfard, M., Ghosh, R., Thundat, T., & Kumar, A. (2016). Dynamics of bacterial streamers induced clogging in microfluidic devices. *Lab on a Chip*, *16*(21), 4091–4096. https://doi.org/10.1039/C6LC01055E

Horsfield, K., & Cumming, G. (1968). Morphology of the bronchial tree in man. *Journal of Applied Physiology*, *24*(3), 373–383. https://doi.org/10.1152/jappl.1968.24.3.373

Hydrophilic Polyester Track Etch (PETE) Membranes Specification. (2016). https://www.sterlitech.com/polyester-membrane-filter-pet0213100.html

Kim, K. P., Kim, Y.-G., Choi, C.-H., Kim, H.-E., Lee, S.-H., Chang, W.-S., & Lee, C.-S. (2010). In situ monitoring of antibiotic susceptibility of bacterial biofilms in a microfluidic device. *Lab on a Chip*, *10*, 3296–3299.

Lebeaux, D., Chauhan, A., Rendueles, O., & Beloin, C. (2013). From in vitro to in vivo models of bacterial biofilm-related infections. *Pathogens*, *2*, 288–356.

Liu, N., Skauge, T., Landa-Marbán, D., Hovland, B., Thorbjørnsen, B., Radu, F. A., Vik, B. F., Baumann, T., & Bødtker, G. (2019). Microfluidic study of effects of flow velocity and nutrient concentration on biofilm accumulation and adhesive strength in the flowing and no-flowing microchannels. *Journal of Industrial Microbiology and Biotechnology*, *46*(6), 855–868. https://doi.org/10.1007/s10295-019-02161-x

Maurice, N. M., Bedi, B., & Sadikot, R. T. (2018). *Pseudomonas aeruginosa* biofilms: Host response and clinical implications in lung infections. *American Journal of Respiratory Cell and Molecular Biology*, *58*(4), 428–439. https://doi.org/10.1165/rcmb.2017-0321TR

Nucci, G., Suki, B., & Lutchen, K. (2003). Modeling airflow-related shear stress during heterogeneous constriction and mechanical ventilation. *Journal of Applied Physiology*, *95*(1), 348–356. https://doi.org/10.1152/japplphysiol.01179.2001

Ohashi, A., & Harada, H. (1994). Adhesion strength of biofilm developed in an attached-growth reactor. *Water Science and Technology*, *29*(10-11), 281–288. https://doi.org/10.2166/wst.1994.0771

Peeters, E., Nelis, H. J., & Coenye, T. (2008). Comparison of multiple methods for quantification of microbial biofilms grown in microtiter plates. *Journal of Microbiological Methods*, *72*(2), 157–165. https://doi.org/10.1016/j.mimet.2007.11.010

Ranganathan, V. (2014). Biofilms: Microbial cities of scientific significance. *Journal of Microbiology & Experimentation*, *1*(3), 84–98. https://doi.org/10.15406/jmen.2014.01.00014

Rühsa, P. A., Böckera, L., Inglisb, R. F., & Fischera, P. (2014). Studying bacterial hydrophobicity and biofilm formation at liquid–liquid interfaces through interfacial rheology and pendant drop tensiometry. *Colloids and Surfaces B: Biointerfaces*, *117*, 174–184. https://doi.org/10.1016/j.colsurfb.2014.02.023

Rutter, P., Dazzo, F., Freter, R., Gingell, D., Jones, G., Kjelleberg, S., & Robb, I. (1984). Mechanisms of adhesion, In K. C. Marshall. (Eds.), *Microbial adhesion and aggregation*, (pp. 4–19). Springer.

Scheuerman, T. R., Camper, A. K., & Hamilton, M. A. (1998). Effects of substratum topography on bacterial adhesion. *Journal of Colloid and Interface Science*, *208*(1), 23–33. https://doi.org/10.1006/jcis.1998.5717

Schwartz, K., Stephenson, R., Hernandez, M., Jambang, N., & Boles, B. R. (2010). The use of drip flow and rotating disk reactors for *Staphylococcus aureus* biofilm analysis. *Journal of Visualized Experiments*, (46), e2470, https://doi.org/10.3791/2470

Stewart, P. S. (2002). Mechanisms of antibiotic resistance in bacterial biofilms. *International Journal of Medical Microbiology*, *292*(2), 107–113. https://doi.org/10.1078/1438-4221-00196

Stewart, P. S. (2003). Diffusion in biofilms. *Journal of Bacteriology*, *185*(5), 1485–1491. https://doi.org/10.1128/JB.185.5.1485-1491.2003

Stoodley, P., Cargo, R., Rupp, C. J., Wilson, S., & Klapper, I. (2002). Biofilm material properties as related to shear-induced deformation and detachment phenomena. *Journal of Industrial Microbiology & Biotechnology*, *29*(6), 361–367. https://doi.org/10.1038/sj.jim.7000282

Stoodley, P., Debeer, D., & Lewandowski, Z. (1994). Liquid flow in biofilm systems. *Applied and Environmental Microbiology*, *60*(8), 2711–2271. https://doi.org/10.1128/aem.60.8.2711-2716

Stoodley, P., Dodds, I., Boyle, J. D., & Lappin-Scott, H. M. (1998). Influence of hydrodynamics and nutrients on biofilm structure. *Journal of Applied Microbiology*, *85*(S1), 19S–28S. https://doi.org/10.1111/j.1365-2672.1998.tb05279.x

Strange, R., & Scott, P. (2005). Plant disease: A threat to global food security. *Annual Review of Phytopathology*, *43*, 83–116. https://doi.org/10.1146/annurev.phyto.43.113004.133839

Thieme, L., Hartung, A., Tramm, K., Klinger-Strobel, M., Jandt, K. D., Makarewicz, O., & Pletz, M. W. (2019). MBEC versus MBIC: The lack of differentiation between biofilm reducing and inhibitory effects as a current problem in biofilm methodology. *Biological Procedures Online*, *21*(18), 18. https://doi.org/10.1186/s12575-019-0106-0

Toyofuku, M., Inaba, T., Kiyokawa, T., Obana, N., Yawata, Y., & Nomura, N. (2016). Environmental factors that shape biofilm formation. *Bioscience, Biotechnology, and Biochemistry*, *80*, 7–12. https://doi.org/10.1080/09168451.2015.1058701

Vandevivere, P., & Baveye, P. (1992). Effect of bacterial extracellular polymers on the saturated hydraulic conductivity of sand columns. *Applied and Environmental Microbiology*, *58*(5), 1690–1698. https://doi.org/10.1128/AEM.58.5.1690-1698.1992

Vieira, M. J., Melo, L. F., & Pinheiro, M. M. (1993). Biofilm formation: Hydrodynamic effects on internal diffusion and structure. *Biofouling*, *7*(1), 67–80. https://doi.org/10.1080/08927019309386244

Williams, D. L., & Bloebaum, R. D. (2010). Observing the biofilm matrix of *Staphylococcus epidermidis* ATCC 35984 grown using the CDC biofilm reactor. *Microscopy and Microanalysis*, *16*(2), 143–152. https://doi.org/10.1017/S143192760999136X

Woodworth, B. A., Tamashiro, E., Bhargave, G., Cohen, N. A., & Palmer, J. N. (2008). An in vitro model of *Pseudomonas aeruginosa* biofilms on viable airway epithelial cell monolayers. *American Journal of Rhinology*, *22*(3), 235–238. https://doi.org/10.2500/ajr.2008.22.3178

Yang, S., & Lewandowski, Z. (1995). Measurement of local mass transfer coefficient in biofilms. *Biotechnology and Bioengineering*, *48*(6), 737–744. https://doi.org/10.1002/bit.260480623

Ye, Z., Silva, D. M., Traini, D., Young, P., Cheng, S., & Ong, H. X. (2022). An adaptable microreactor to investigate the influence of interfaces on *Pseudomonas aeruginosa* biofilm growth. *Applied Microbiology and Biotechnology*, *106*, 1–11.

How to cite this article: Zhang, Y., Silva, D. M., Young, P., Traini, D., Li, M., Ong, H. X., & Cheng, S. (2022). Understanding the effects of aerodynamic and hydrodynamic shear forces on *Pseudomonas aeruginosa* biofilm growth. *Biotechnology and Bioengineering*, 119, 1483–1497. https://doi.org/10.1002/bit.28077